

We are IntechOpen, the world's leading publisher of Open Access books Built by scientists, for scientists

6,900

Open access books available

186,000

International authors and editors

200M

Downloads

Our authors are among the

154

Countries delivered to

TOP 1%

most cited scientists

12.2%

Contributors from top 500 universities



WEB OF SCIENCE™

Selection of our books indexed in the Book Citation Index
in Web of Science™ Core Collection (BKCI)

Interested in publishing with us?
Contact book.department@intechopen.com

Numbers displayed above are based on latest data collected.
For more information visit www.intechopen.com



Design of a Low-Cost Permanent Synchronous Machine for Isolated Wind Conversion Systems

Florin-Nicolae Jurca

Additional information is available at the end of the chapter

<http://dx.doi.org/10.5772/62817>

Abstract

The chapter deals with the theoretical analysis of two configurations of low-cost permanent synchronous generator (PMSG), suitable for small rating, direct driven applications, such as small- and microscale wind power plants. The first structure is a permanent magnet claw-pole synchronous generator (PMCPSPG) to be used in an isolated microwind power plants with installed power around few hundred Watts. A permanent magnet synchronous machine with outer rotor (PMSMOR) is the second presented structure, suitable for small wind system with installed power between 2 and 5 kW. In order to obtain the optimal value of the main geometric dimensions of the generators, an optimization procedure, based on Hooke-Jeeves method, was implemented for all the considered structures.

Keywords: permanent synchronous machine, low-cost permanent magnet, small-scale wind power plants, direct-driven, optimization

1. Introduction

Wind turbines are widely used as a pollution-free and renewable source in order to supplement other electricity generators. Wind power technology has developed remarkably during the latest decade. Due to its flexibility, it can be used practically anywhere.

Small wind turbines have been used to generate electricity for rural farms or others remote buildings which do not have the possibility to connect to a main power supply. The increasing demand in recent years for clean and affordable energy will lead without doubt to a wider use of the small turbines for urban area.

The technology of the generator system in small wind turbine can be classified into direct drive and the geared technology concepts. The geared generator system has the advantages in terms of the cost, size, and weight. The direct-drive generator system is superior in terms of efficiency, reliability, and maintenance problem [1]. Because in direct drive generator technology is necessary a high number of poles, accordingly with a big weight, the permanent synchronous machine (PMS) have the advantages of comparing to other machines of being robust in construction, very compact in size, not requiring an additional power supply for magnetic field excitation [2]. One problem of this generator is the cost, especially when the permanent magnet is neodymium, because in the last years its price is continuously increasing. The solution is to use low-cost permanent magnets, such as ferrites and alnico. These materials are reasonably easy to find [3]. Usually, the performances of electrical machines with low-cost permanent magnets are lower comparative with the same machines using neodymium magnet. In order to keep the generator with low-cost permanent magnet feasible, more attention is necessary in design and optimization procedure. So, the challenge for small- and microscale wind power plants is to find a solution to maintain the lower costs of systems (e.g, generator) in conditions of reliability and the high value of efficiency.

This is the motivation of this research work. For that, two configurations of low-cost PMSG suitable for direct drive in wind power applications will be studied from the theoretical point of view.

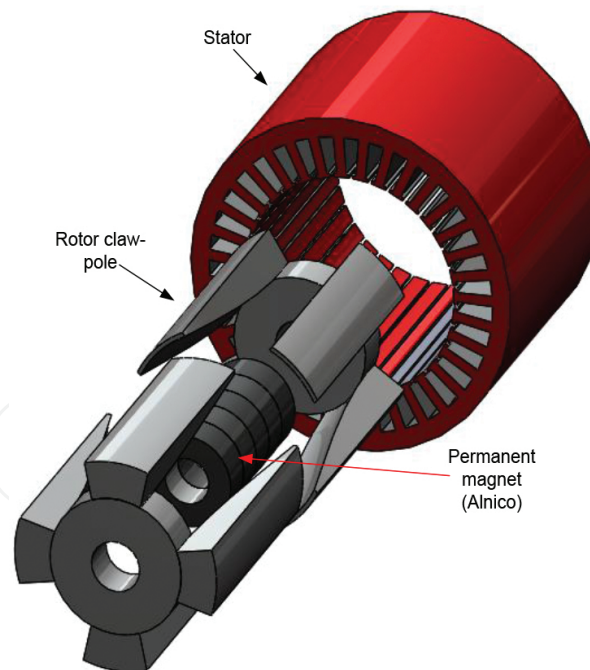


Figure 1. The PMCPMSG topology.

The first structure is a permanent magnet claw-pole synchronous generator (PMCPMSG) obtained usually from the conversion of an induction or a synchronous conventional machine (see **Figure 1**), suitable for isolated microwind power plants with installed power around few

hundred Watts. A permanent magnet synchronous machine with outer rotor (PMSMOR) is the second presented structure (see **Figure 2**), suitable for small wind system with installed power between 2 and 5 kW. Hence in this chapter, an exhaustive approach will be presented by going through all the phases in the development cycle of special topologies of low-cost permanent magnet synchronous machine.

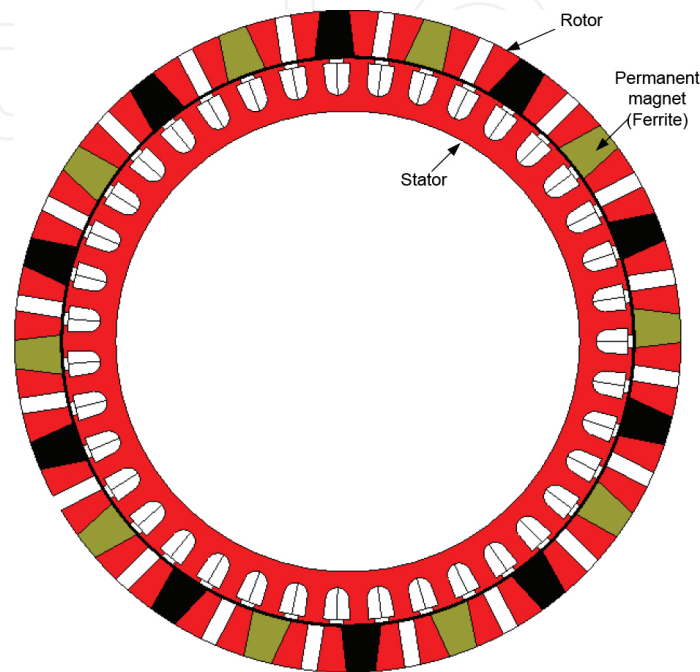


Figure 2. The PMSMOR topology.

2. Design and optimization of the studied electrical machines

2.1. Design of PMCPSPG

The objective of the present subchapter was the design and optimization of a three-phase PMCPSPG, driven by a small wind turbine with the following set of key parameter: $s_N=180$ apparent power (VA); rated phase voltage $u_N=100$ (V); rated speed $n_N=750$ rpm; pole pair number $p=4$; permanent magnet-type Alnico. In addition, several constraints must be met such as limited size, low weight, and low torque ripple content.

The analytical procedure includes the following topics: analysis of the specifications, selection of the topology and of the active and passive materials, dimensioning of the geometry, parameter and performance calculation, choice of the manufacturing technologies, and cost prediction.

For the given output power and operating speed, the PMCPSPG main dimensions may be determined using the output power equation, based on specific magnetic and electric loads [4]. The inner stator diameter results as follows:

$$D_{is} = \sqrt[3]{\frac{60 \cdot S_N}{C \cdot n_N \cdot \lambda}} \quad (1)$$

with D_{is} —the stator inner diameter; C —machine constant; and λ —geometrical form factor. For PMGPSG, the machine constant could be written as:

$$C = \frac{\pi^3}{2\sqrt{2}} \cdot k_w \cdot \alpha_i \cdot A \cdot B_g \quad (2)$$

with A —electrical load (between 30 and 80 k_A/m for indirect air cooling); B_g —magnetic load (0.4...0.8 T for machines using Alnico); k_w —winding factor; and α_i —pole pitch coverage coefficient [the ratio between the rotor pole width (b_{pr}) and the rotor pole pitch (τ_r)] [4]. As a starting point, due to the special configuration of the rotor, the values for k_w (0.92... 0.966) and α_i (0.6...0.9) were chosen according to [4, 5] for a permanent magnet synchronous machine with rotor salient poles and single-layer fractional windings (see **Figure 3**).

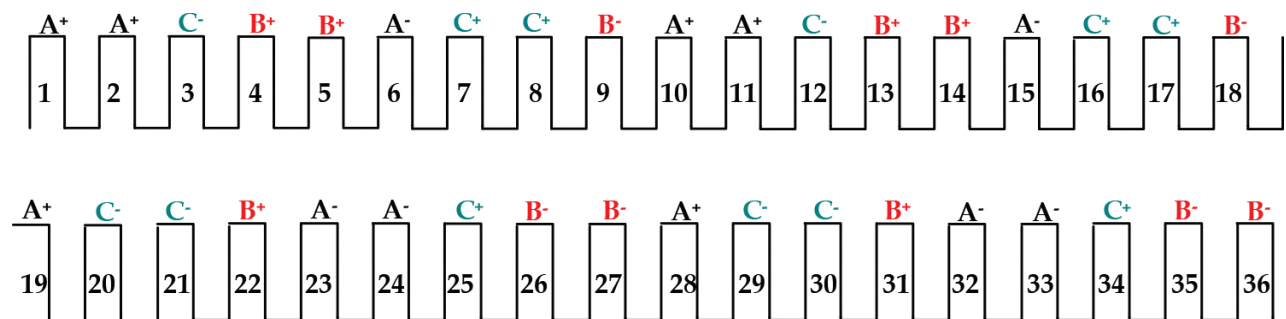


Figure 3. Stator winding of PMGPSG.

The lamination stack length results as follows:

$$l_{Fe} = \lambda \cdot D_{is} \quad (3)$$

Computation of the rotor outer diameter gives:

$$D_r = D_{is} - 2 \cdot g \quad (4)$$

with g —air-gap length.

Due to fault tolerance consideration and the fractional number of slots per pole and phase ($q = 1.5$), a single-layer fractional winding was chosen. The rms value of the phase electromotive force (emf) is given by [6]:

$$E_{ph_rms} = \pi \cdot \sqrt{2} \cdot f \cdot k_w \cdot W_1 \cdot l_{Fe} \cdot \frac{\pi \cdot D_{is}}{2 \cdot p} \cdot B_{g_av} \quad (5)$$

with w_1 —number of turns per phase, p —number of pole pairs, and B_{g_av} —average magnetic load.

Starting from the geometric dimensions of the stator and the electrical parameters of the generator, we will obtain from the winding design algorithm, the winding connection diagram (see **Figure 3**), the number of turns per phase (W_1), the area of the wire cross section (S_c), the number of turns per slot (n_c), and the number of parallel current paths (a) [4].

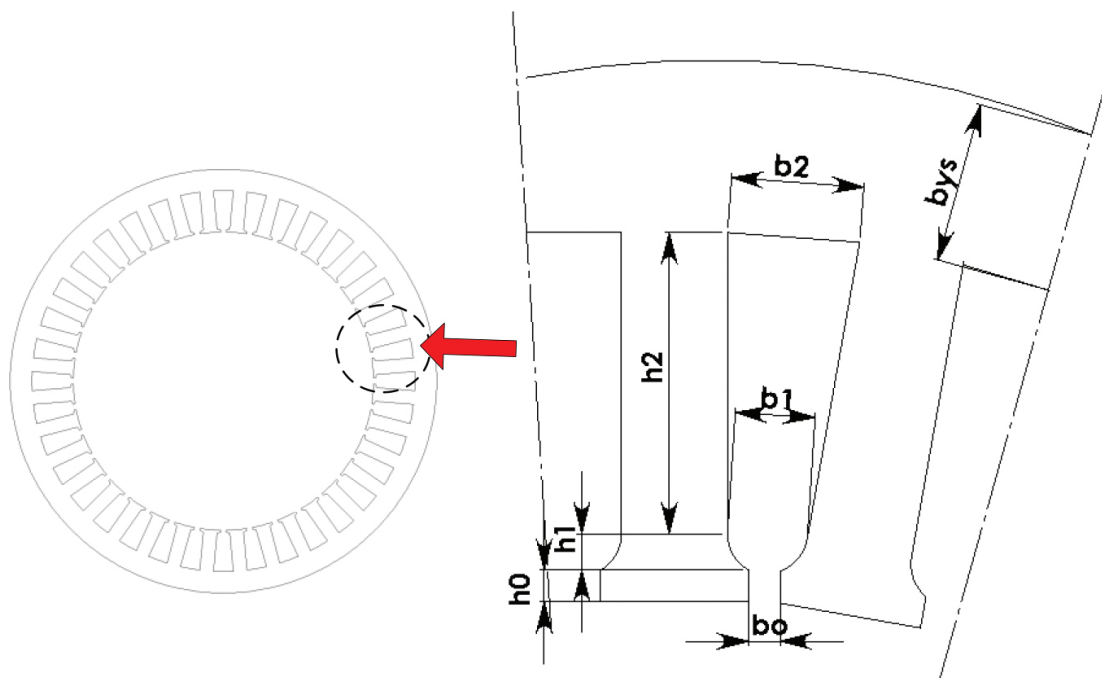


Figure 4. Stator slot geometry.

For the stator slot a trapezoidal cross section was chosen (see **Figure 4**). Its dimensions are derived from the slot area:

$$A_{slot} = \frac{n_c \cdot S_c}{k_{fill}} = b_0 \cdot h_0 + \frac{b_1 + b_0}{2} \cdot h_1 + \frac{b_2 + b_1}{2} \cdot h_2 \quad (6)$$

with $k_{fill} = 0.36 \dots 0.55$ and b_{ts} —the stator tooth width:

$$b_{ts} = \frac{\pi \cdot D_{is} \cdot B_{g_av}}{Q_s \cdot B_{ts_av}} \quad (7)$$

with B_{ts_av} – average flux density in stator tooth, usually between 0.8 and 1.2 T according to [5, 7]. Finally, choosing the values for the slot opening, tooth tip height, fixing wedge height [4], the stator slot, and tooth dimensions can be computed. The width of the stator yoke results as follows [6]:

$$b_{ys} = \frac{\pi \cdot D_{is} \cdot B_{g_av}}{2 \cdot p \cdot B_{ys_av}} \quad (8)$$

with B_{ys_av} – average flux density in stator yoke, usually between 0.6 and 1 T according to [5, 7].

Thus, the outer stator diameter results as follows:

$$D_{os} = D_{is} + 2 \cdot (h_{ts} + h_{ys}) \quad (9)$$

with h_{ts} – the stator tooth height and h_{ys} – the stator yoke height.

The rotor steel plate carrying 4 claw poles and its dimensions to be computed are shown in **Figure 5**.

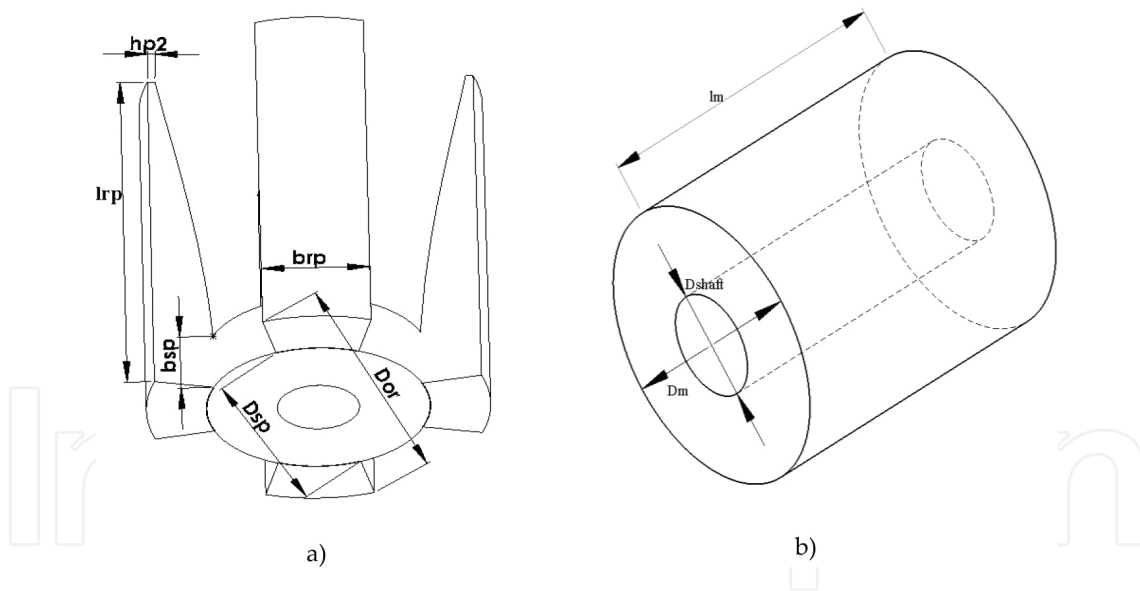


Figure 5. Rotor geometry: (a) claw-pole structure, (b) permanent magnet.

For reducing the leakage flux between two claw poles, the rotor claw-pole width value is given by:

$$b_{pr} = (0.6 \dots 0.8) \cdot \tau_r \quad (10)$$

The height of the rotor pole tip:

$$h_{p2} = (2 \dots 4) \cdot g \quad (11)$$

The length of the rotor pole should be smaller than the rotor length:

$$l_{rp} = (0.85 \dots 0.95) \cdot l_{Fe} \quad (12)$$

As the permanent magnet will be accommodated between the two steel plates, its length can be computed as:

$$l_m = l_{Fe} - 2 \cdot b_{sp} - 2 \cdot b_{wedge} \quad (13)$$

with $b_{wedge} = 3.5$ mm.

Considering the average value of the magnetic field density in the air-gap, the average value of the magnetic field density in different parts of the machine (B_x) is calculated as [6]:

$$B_{x_av} = \frac{k_x \cdot \pi \cdot D_{is} \cdot l_{Fe} \cdot B_{g_av}}{2 \cdot p \cdot A_x} \quad (14)$$

with A_x the average area of the cross section of the x part of the machine (stator teeth and yoke, rotor claw poles, rotor steel plates, etc) and k_x a coefficient giving the percent of the air-gap magnetic field that is crossing the x part of the machine [8].

2.1.1. Steady-state parameters and losses computation of PMCPSPG

The d-q model of the generator is characterized by the synchronous reactance' defined on direct and quadrature axis, X_d and X_q , respectively. The d-q reactance's are given as:

$$\begin{aligned} X_d &= \omega_1 \cdot L_d = \omega_1 \cdot (L_{md} + L_{s\sigma}) \\ X_q &= \omega_1 \cdot L_q = \omega_1 \cdot (L_{mq} + L_{s\sigma}) \end{aligned} \quad (15)$$

with ω_1 the rotor electrical speed, L_d and L_q the direct and quadrature axis corresponding synchronous inductances [8], given as the sum between the corresponding magnetizing inductances, L_{md} and L_{mq} and the stator leakage inductance, $L_{s\sigma}$. Simplified formulae for the magnetizing inductances were derived as [8]:

$$\begin{aligned}
 L_{md} &= L_m \cdot \frac{k_d \cdot k_f}{1 + k_{sd}} \\
 L_{mq} &= L_m \cdot \frac{k_q \cdot k_f}{1 + k_{sq}}
 \end{aligned}
 \tag{16}$$

with L_m —the magnetizing inductance [8], k_d and k_q —the armature reaction coefficients, k_f —the form factor, and k_{sd} and k_{sq} —the saturation factors corresponding to direct and quadrature axis, respectively.

The magnetizing inductance of the three-phase PMCPSPG was computed [4]:

$$L_m = \frac{3 \cdot D_{is}}{\pi \cdot p \cdot g_{ef}} \cdot \mu_0 \cdot l_{Fe} \cdot (k_w \cdot W_1)^2
 \tag{17}$$

with g_{ef} —the effective air-gap, including the Carter factor [4]. The Carter factor was calculated considering both the stator and rotor Carter factors [9]. The expressions for the coefficients in [Eq. (16)] correspond to the ones presented in [10].

Stator leakage inductance was calculated for the stator slot geometry shown in **Figure 3** as the sum of four main components [4]: air-gap leakage inductance, slot leakage inductance, tooth tip leakage inductance, and end-winding leakage inductance. The phase resistance can be computed with the formula [4, 11].

$$R_s = \frac{W_1 \cdot l_c}{\sigma \cdot a \cdot S_c}
 \tag{18}$$

with l_c —average length of a turn in a coil and σ —conductivity of the conductor material.

Next, the losses and efficiency can be determined. The main losses of the PMCPSPG [8] are as follows:

$$P_{losses} = P_{Joule} + P_{Fe} + P_{mech}
 \tag{19}$$

where P_{mech} —mechanical losses (can be approximated at 1%, as a starting point). Iron losses are the sum of hysteresis (P_{hyst}) and eddy current ($P_{eddy_currents}$) for stator and rotor cores and the claw-pole surface (P_{scwp}) losses. The losses can be computed considering the general expression [4]:

$$\begin{aligned}
 P_{hyst/eddy_currents} &= C_{mat} \cdot f^{af} \cdot B^{aB} \cdot G \\
 P_{scwp} &= 2 \cdot p \cdot S_{cwp} \cdot k_{cp} \cdot f^{1.5} \cdot B_{g_av}^2
 \end{aligned}
 \tag{20}$$

where a_f and a_B —material empirical constants than can be determinate from curve-fitting the losses for a wide range of “ f ” (frequency) and B values; k_{cp} —a factor dependent on the claw-pole material and machine Carter factor; and G —the weight of the considered part of the machine [6].

Thus, the efficiency of the machine can be written as:

$$\eta = \frac{P_N}{P_N + P_{losses}} \quad (21)$$

with $P_N = S_N \cdot \cos\phi$.

After, the designing process, the following results have been obtained, see **Table 1**.

Parameter	PMCPSTG
Output power (W)	150
Rated speed (rpm)	750
Phase voltage (V)	50
Number of phases (-)	3
Number of pole pairs (-)	4
Number of slots	36
Stator outer diameter (mm)	145
Stator inner diameter (mm)	95
Rotor pole width (mm)	29
Rotor pole length (mm)	105
Rotor pole base height (mm)	15
Steel plate radius (mm)	31
Rotor pole tip height (mm)	21
Permanent magnet diameter (mm)	60
Residual flux density—Alnico 8 (T)	0.9
Coercive force—Alnico 8 (kA/m) [11]	115
Rated current (A)	1
Losses (W)	81
Efficiency (%)	70

Table 1. Obtained results for the designed PMCPSTG.

2.2. Design of PMSMOR

The dimensioning procedure was applied for the following set of key parameters: P_{out} —3 kW (estimated); rated phase voltage u_N —220 (V); rated speed n_N —500 rpm; pole pair number p —10.

By neglecting the leakage reactance and for a certain number of phases (m), phase current $i(t)$, and induced emf $e(t)$, we obtain the output power of an electrical machine [13]:

$$P_{out} = \eta \cdot \frac{m}{T} \cdot \int_0^T e(t) \cdot i(t) dt = \eta \cdot m \cdot k_p \cdot E_{max} \cdot I_{max} \quad (22)$$

where T is the period of one cycle of emf, E_{max} is the peak value of the emf, I_{max} is peak value of the phase current, k_p is the power coefficient, and η is the estimated efficiency. The peak value of the emf is expressed by introducing the electromotive force coefficient, k_E [13]:

$$E_{max} = k_E \cdot W_1 \cdot B_g \cdot D_g \cdot l_m \cdot \frac{f}{p} \quad (23)$$

with D_g —air-gap diameter.

By introducing a geometric coefficient, $k_L = L_m/D_g$, and a current coefficient (related to its wave form) $k_i = I_{max}/I_{rms}$, and defining the phase load ampere-turns:

$$A = \frac{2}{\pi} \cdot W_1 \cdot \frac{I_{rms}}{D_g} \quad (24)$$

it is possible to define the air-gap diameter of the machine [13]:

$$D_g = \sqrt[3]{\frac{2 \cdot p \cdot P_{out}}{\pi \cdot m \cdot A \cdot k_E \cdot k_i \cdot k_p \cdot k_L \cdot \eta \cdot B_g \cdot f}} \quad (25)$$

The height of the permanent magnet results as follows:

$$h_m = \frac{\pi \cdot D_{ir} \cdot B_g}{2 \cdot p \cdot B_m} \quad (26)$$

with $B_m = 0.405 \text{ T}$ (for permanent magnet type: ferrite) and interior diameter of rotor: $D_{ir} = D_g + g$.

Using Eq. (16), the dimensions of different parts of the rotor (permanent magnet width, rotor pole width, air barrier width) are calculated (see **Figures 6, 7**). All the other stator geometric parameters will be computed based on air-gap diameter, as for conventional synchronous machine. Thus, the performances of the generator will be determined with conventional equations [4]. All results after the designing process and the performances obtained are presented in **Table 2**.

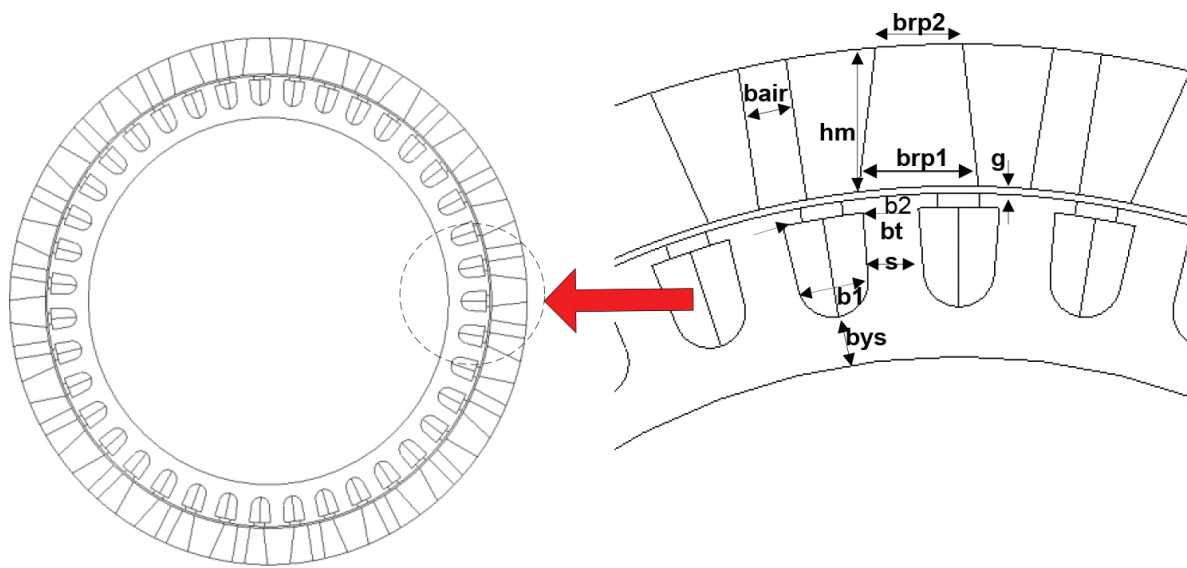


Figure 6. Stator and rotor geometry of PMSMOR.

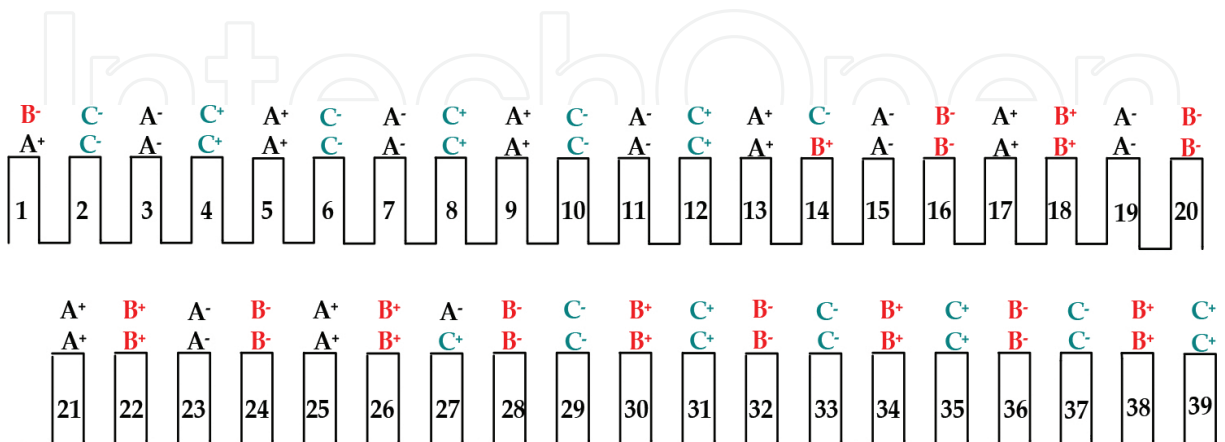


Figure 7. Stator winding of PMSMOR.

Parameter	PMSMOR
Output power (W)	3000
Rated speed (rpm)	500
Phase voltage (V)	220
Number of phases (-)	3
Number of pole pairs (-)	10
Number of slots	39
Stator outer diameter (mm)	248
Stator inner diameter (mm)	202
Rotor outer diameter (mm)	290
Rotor pole height (mm)	21
Rotor pole base width (mm)	5.2
Rotor pole top width (mm)	10.5
Permanent magnet base width (mm)	18
Permanent magnet top width (mm)	13
Residual flux density—Ferrite Y30BH (T)	0.405
Coercive force—Ferrite Y30BH (kA/m) [12]	230
Rated current (A)	5
Losses (W)	500
Efficiency (%)	86

Table 2. Obtained results for the designed PMSMOR.

2.3. Optimization of PMCPSPG and PMSMOR

The influence of different geometrical dimensions on the PMCPSPG and PMSMOR performances can be done by using 3D and 2D, respectively. Despite the fact that the results provided by finite element method (FEA) are accurate and can be very useful in for the optimization of the main geometric dimensions, this approach is highly time-consuming [6]. Hence, in order to reduce the time cycle and the number of iterations, a better solution is to use an optimization based on an analytical algorithm. Due to technological and cost constraints, two available stator laminations with the geometry given in **Figures 3** and **4**, respectively, and the dimensions given in **Tables 1** and **2**, respectively, were chosen.

The optimization of electric machine is a multivariable, nonlinear problem with constraints. To treat problems with constraints is necessary to transform them in unconstrained ones. This can be done, for example, by embedding the constraints in the objective function [6]. The so-called direct search optimization methods fulfill these requirements. Hooke-Jeeves, one direct search method, was selected for the optimization of the presented generators [6, 14]. The main steps in the optimization algorithm are as follows (see **Figure 8**): the choice of the optimization

variables, input of the constraints, the definition of the objective function, objective function calculation, the computation of the main parameters (geometrical and electromagnetic), and the visualization of the obtained result.

For the studied machine, a set of 4 variables ($x_i, i = 1 \dots 4$) for each structures were selected (see **Table 3**). In order to keep the topology, functional limits are set for each variable and specific constraints are set, together with a penalty coefficient for including in the objective function.

The following constraints were considered:

- a. The output power has to be greater or equal to the design specified value.
- b. The air-gap magnetic flux density has to be closed to the specified value.
- c. The stator teeth magnetic flux density has to be closed to the specified value.
- d. The stator lamination geometry remains unchanged.

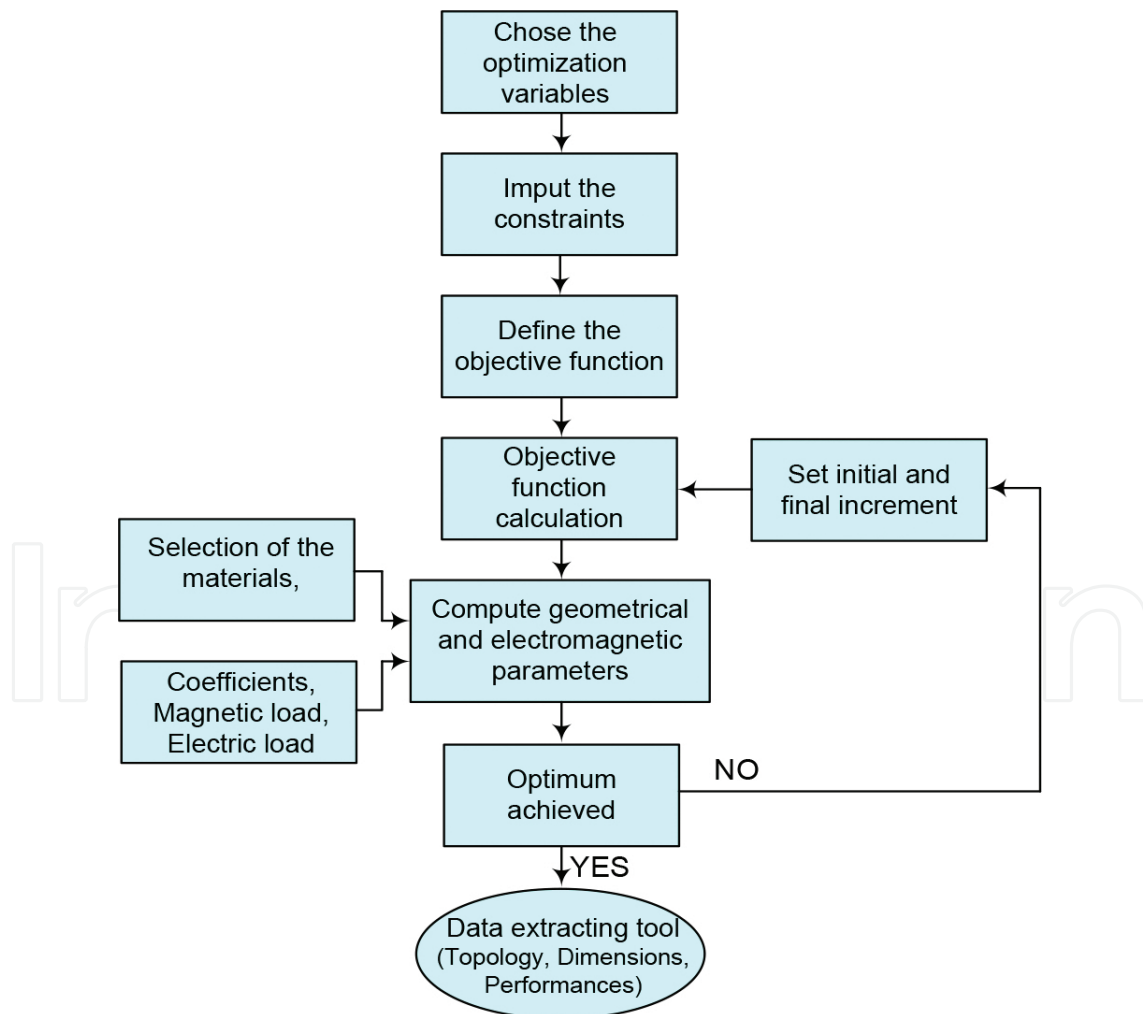


Figure 8. Optimization algorithm.

PMSMOR parameters	Initial value	Boundaries
Rotor pole width b_{rp} (mm)	29	[25.....35]
Rotor pole length l_{pr} (mm)	105	[55.....110]
Rotor pole base height h_{sp} (mm)	15	[10.....20]
Rotor pole to height h_{p2} (mm)	2.5	[1.....3.5]
PMSMOR parameters		
PM base width b_{rp1} (mm)	18	[14.....22]
PM top width b_{rp2} (mm)	13	[10.....16]
Height of the PM on magnetization direction h_m (mm)	21	[18.....23]
Rotor barrier width b_{air} (mm)	6	[5.....8]

Table 3. Optimization variables: initial values and boundaries.

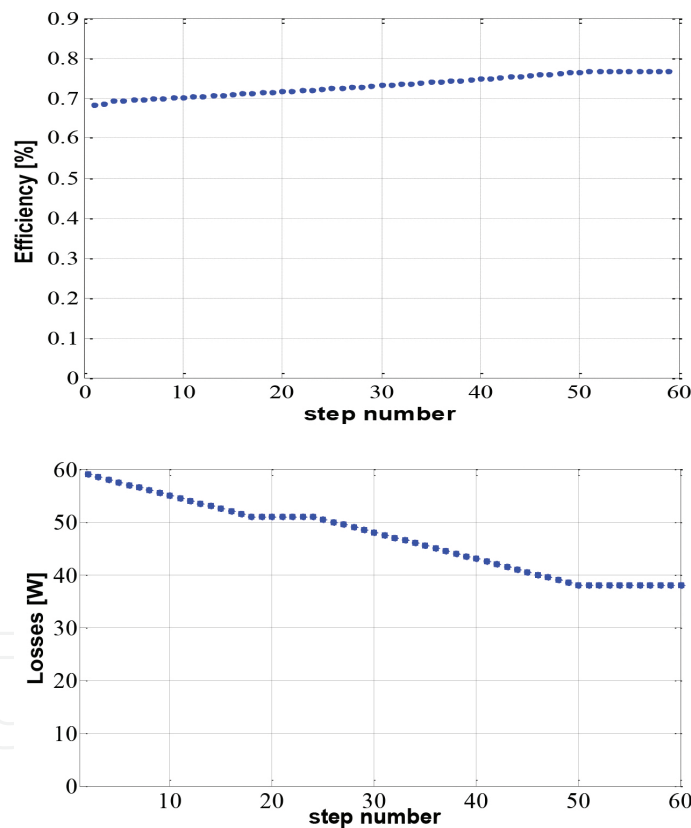


Figure 9. Optimization results of PMCPSPG: efficiency and losses.

For the generators dedicated to microwind and small wind conversion systems, some optimization issues (objective functions) are important: low-cost, maximum generated voltage, and maximum efficiency. The maximum efficiency ($f_1(x_1)$) for the maximum generated voltage ($f_2(x_2)$) was selected as multi-objective optimization function. The chosen multi-objective function is mathematically expressed as [6]:

$$f(x_i) = w_1 \cdot f_1(x_i) + w_2 \cdot f_2(x_i) \quad (27)$$

The iterative process has reached its optimum after 60 steps, the simulation time being 1.26 s. The efficiency and the losses have been plotted in **Figure 9**, while the evolution of the geometric parameters of PMCPSPG has been plotted in **Figure 10**. It can be seen that some parameters presented a low variation, but the length of claw pole presented a high variation around a mean value.

It is obvious that if the geometrical parameters will decrease, the iron losses will decrease too. This is the normal behavior; thus, the efficiency of the generator will increase. For the PMCPSPG, the efficiency of the machine will increase with 8%.

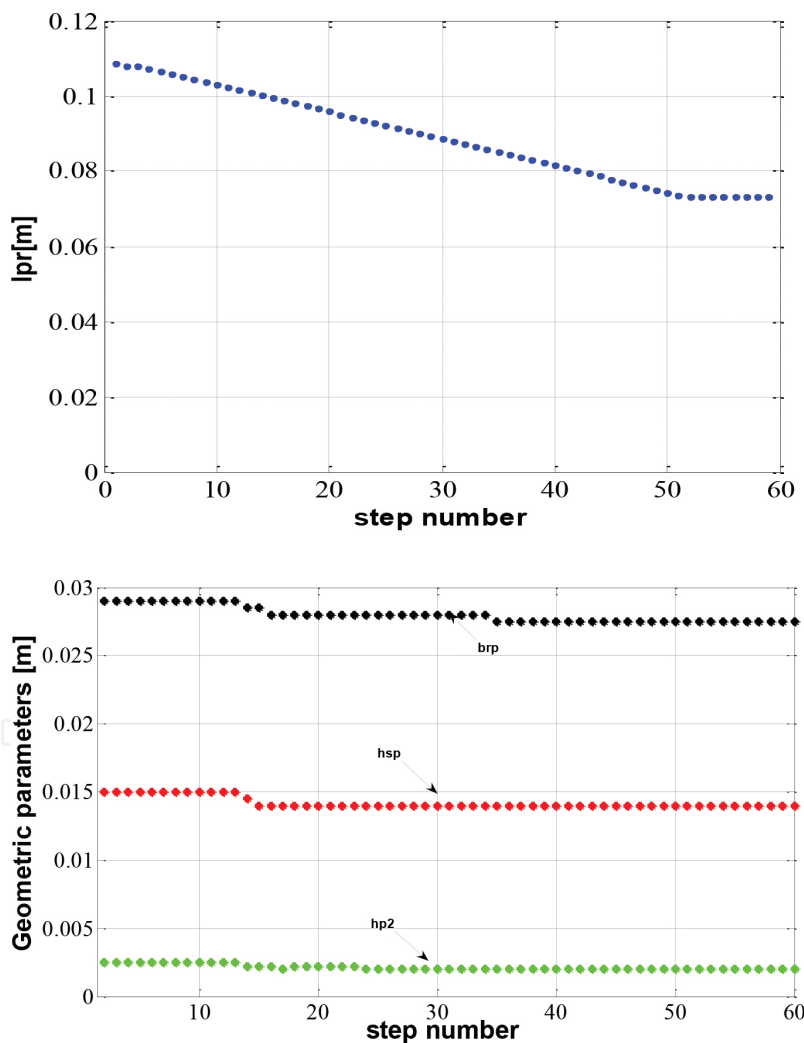


Figure 10. Optimization results of PMCPSPG: evolution of geometrical parameters.

In **Figure 11**, the evolution of efficiency and losses of PMSMOR during the optimization process have been plotted. For this machine, the efficiency increase with decrease of losses due

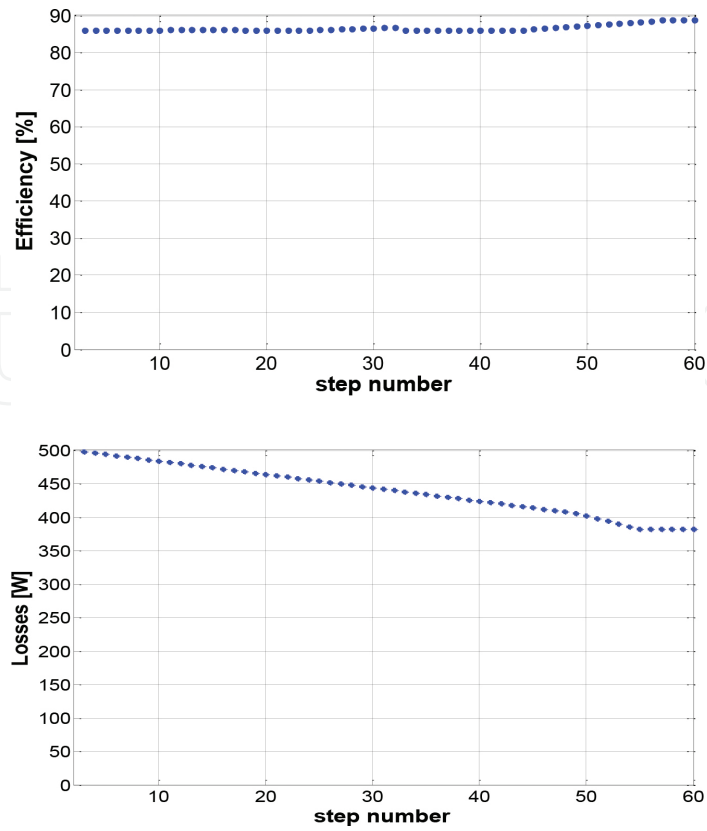


Figure 11. Optimization results of PMSMOR: efficiency and losses.

to changes of geometrical parameters is shown in **Figure 12**. Here, only the permanent magnet dimensions and rotor flux barrier width are presented as a sample. It can be seen that the value of geometrical parameters of permanent magnet is reduced, consequently barrier rotor width increased. The efficiency of the machine has globally increased with 3%.

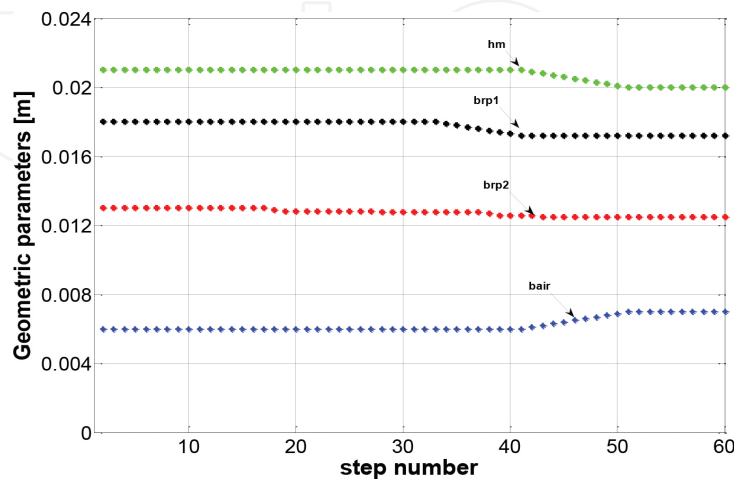


Figure 12. Optimization results of PMSMOR: evolution of geometrical parameters.

PMCPSPG parameters	Initial value	Final value
Rotor pole width b_{rp} (mm)	29	27
Rotor pole length l_{pr} (mm)	105	60
Rotor pole base height h_{sp} (mm)	15	14
Rotor pole to height h_{p2} (mm)	2.5	2
Losses (W)	60	38
Efficiency (%)	0.695	0.78
PMSMOR parameters		
PM base width b_{rp1} (mm)	18	17
PM top width b_{rp2} (mm)	13	12.5
Height of the PM on magnetization direction h_m (mm)	21	20
Rotor barrier width b_{air} (mm)	6	7
Rotor outer diameter (mm)	290	288
Losses (W)	502	384
Efficiency (%)	85.8	89.1

Table 4. Main optimization results, at rated operating point, for both considered topologies.

The resume of the optimized results of the PMCPSPG and PMSMOR are given in **Table 4**.

3. Magnetic field analysis of the studied electrical machines

The magnetic flux density distribution in the electrical machines' core is very important because this affects the voltage waveform, the iron losses, and the efficiency. The finite element method (FEM) is a simple, robust, and efficiently widely used method of obtaining a numerical approximate solution for a given mathematical model of the machine [6]. This analysis has been carried out by using Flux software (2D for PMSMOR and 3D for PMCPSPG).

3.1. Magnetic field analysis of PMCPSPG

Due to the complex three-dimensional structure of claw pole, the magnetic field inside the claw-pole generator needs to be treated as a 3D problem, using 3D module of Flux software [14]. In the case of 3D simulations, high memory resource of computer is necessary. However, they are much time-consuming. In order to reduce this, considering the symmetry of the machine structure, the analysis will be carried out for one pole pair. In the first steps of the analysis, the geometry of the structure was introduced and the mesh was generated. Next, if the previous steps are correct, the solution will be generated. After that, in post-processing stage, the data about magnetic behavior (map of flux density in the stator and rotor core, air-gap flux density distribution) and other performances (induced emfs, cogging torque, etc) of the generators will be computed [6].

The no-load regime for the rated speed was simulated, in order to present the maps of the magnetic flux density in the stator and rotor core (Figure 13).

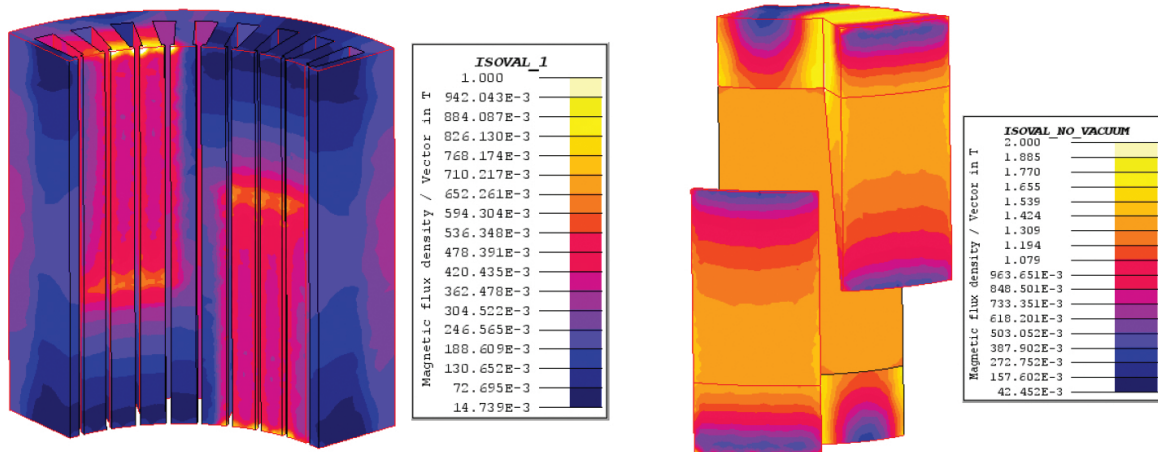


Figure 13. Magnetic flux density map in the stator an rotor core.

It has been observed that in Figure 13, the value of magnetic flux density is very close to the saturation level of the considered steel, especially at the base of the claw pole, where the direction of the flux density is changing. Since due to its complex three-dimensional structure, the rotor claws are usually press-formed out of solid metal or pressed in a die of iron powder [14], magnetic flux density distribution along the radial and axial length of the air-gap obtained in load condition are very useful in order to develop an optimum design in terms of low eddy current losses (Figures 14, 15).

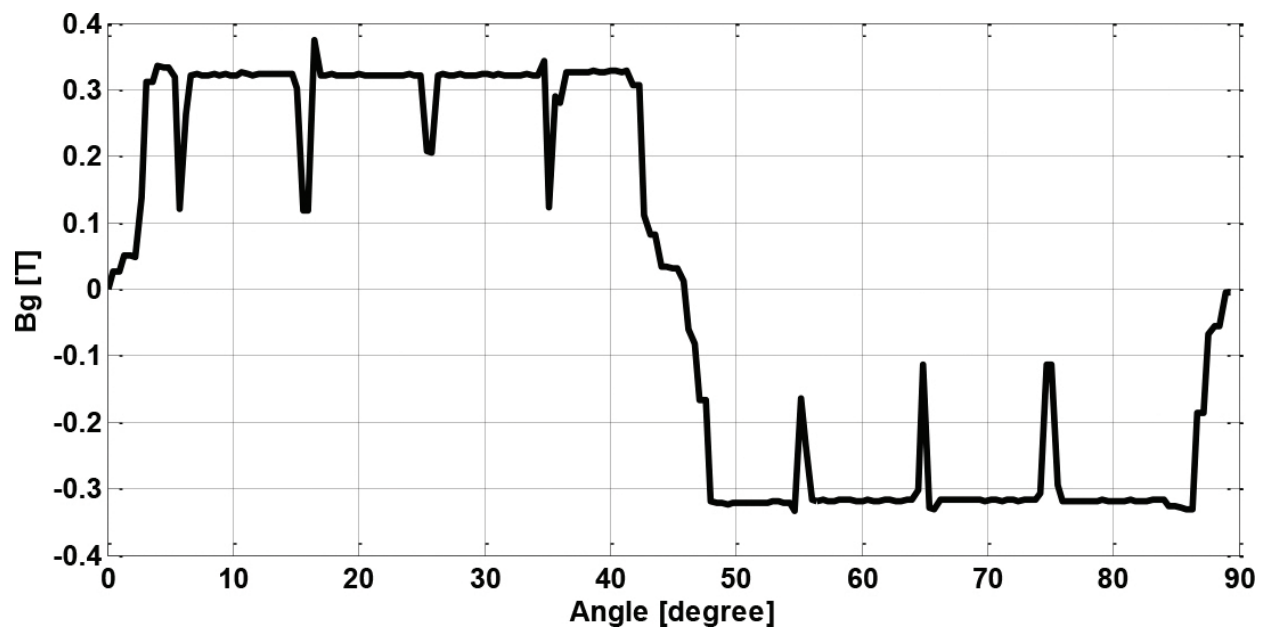


Figure 14. Magnetic field distribution along the radial air-gap.

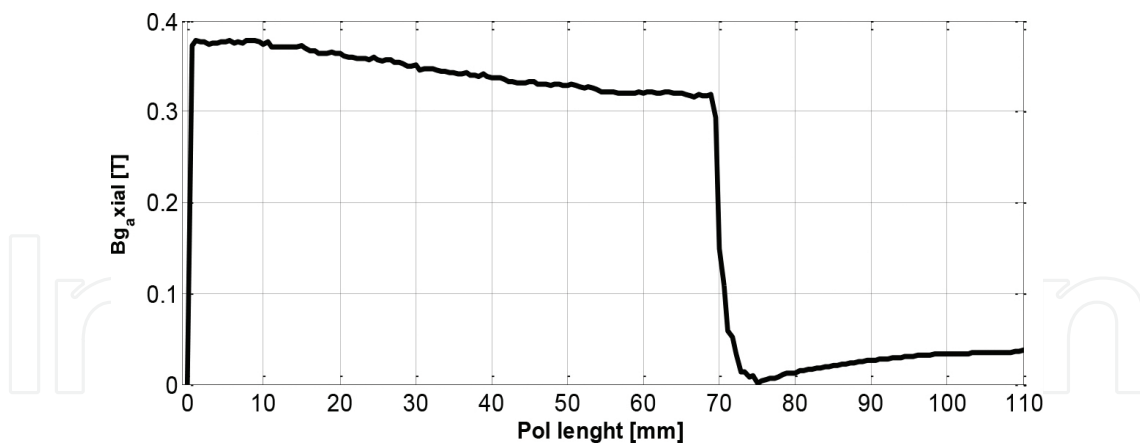


Figure 15. Magnetic field distribution along the axial air-gap.

The wave depicted in **Figure 14** shows maximum values when the air-gap is minimum and minimum values when the air-gap is maximum. As it can be noted that the flux density under each rotor pole has the same value, the peaks corresponding to the four stator teeth overlapped with one rotor pole.

The obtained voltage and axis torque in load condition are shown in **Figures 16** and **17**, respectively. It can be observed that the waveform of voltage is slightly deformed due to the shape of the claw poles. In this case, a further optimization of the shape of the claw poles can be achieved, but this involves a supplementary cost in manufacturing. For the structure of PMCPSPG presented in this chapter, a supplementary optimization of the shape of the claw poles is not necessary in the context of the considered application (isolated microwind power plants with installed power around few hundred Watts).

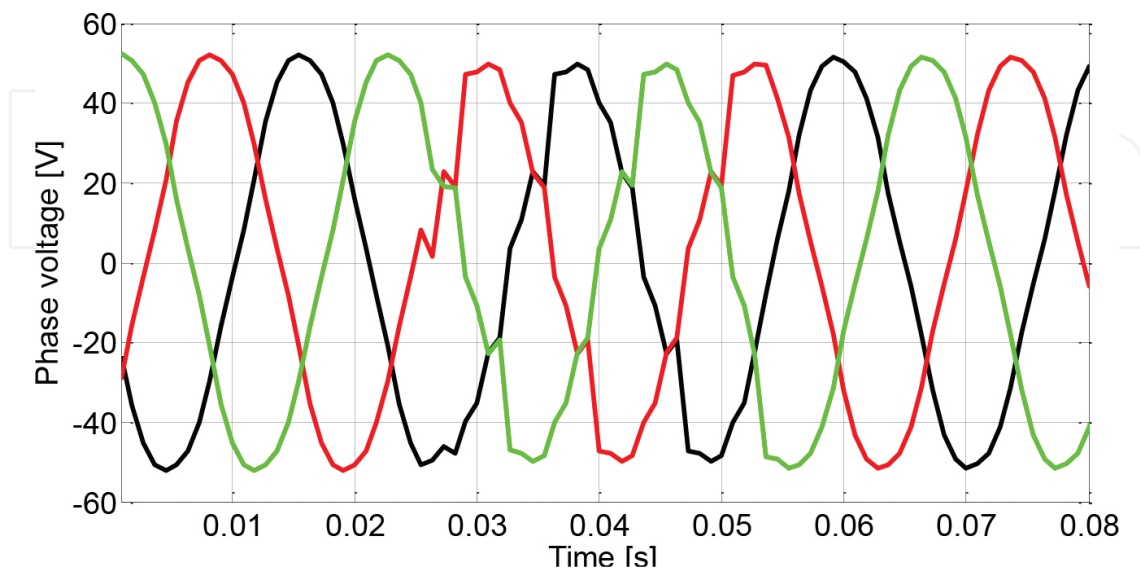


Figure 16. Computed voltage (rms value) in load condition.

The axis torque is obtained based on rated current (1 A). Also, the torque ripple is 15.7%. In this context, no strategy to reduce the torque ripple was adopted.

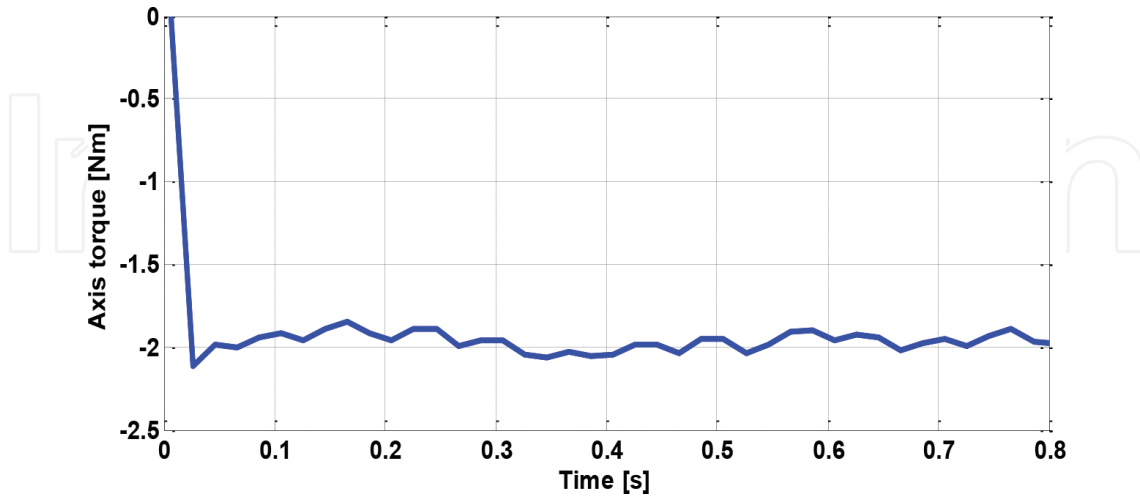


Figure 17. Axis torque in generator regime.

3.2. Magnetic field analysis of PMSMOR

Due to configuration of PMSMOR, the numerical computation has been carried out by using Flux 2D. In order to obtain the map of magnetic flux density distribution in the stator and rotor core and its distribution in air-gap the FEM analysis, in no-load condition, this generator regime is employed at rated speed (500 min^{-1}).

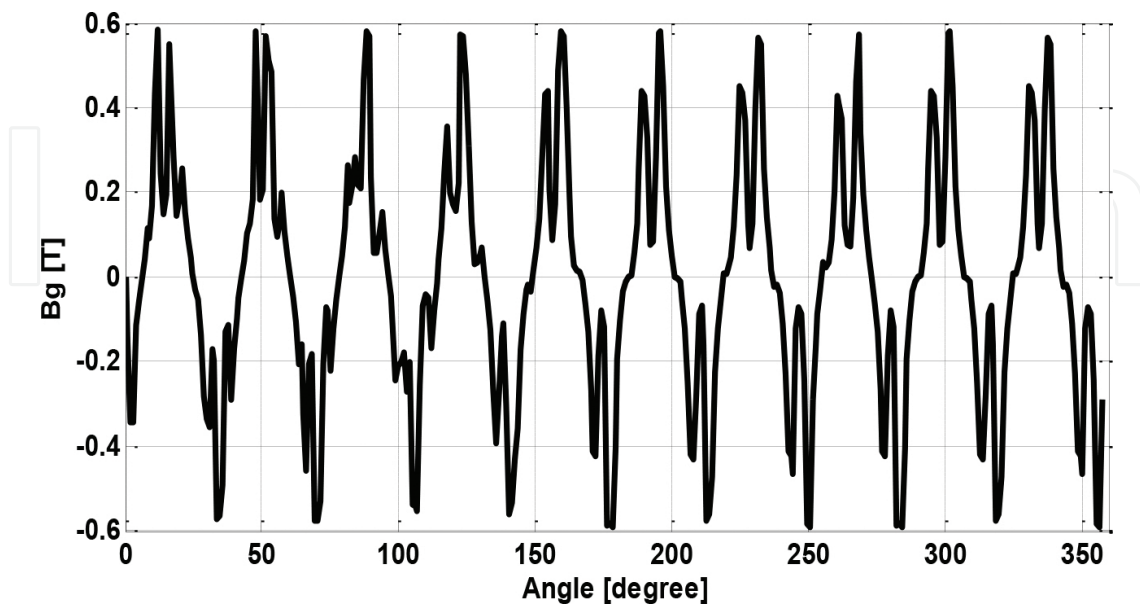


Figure 18. Magnetic field distribution in the air-gap.

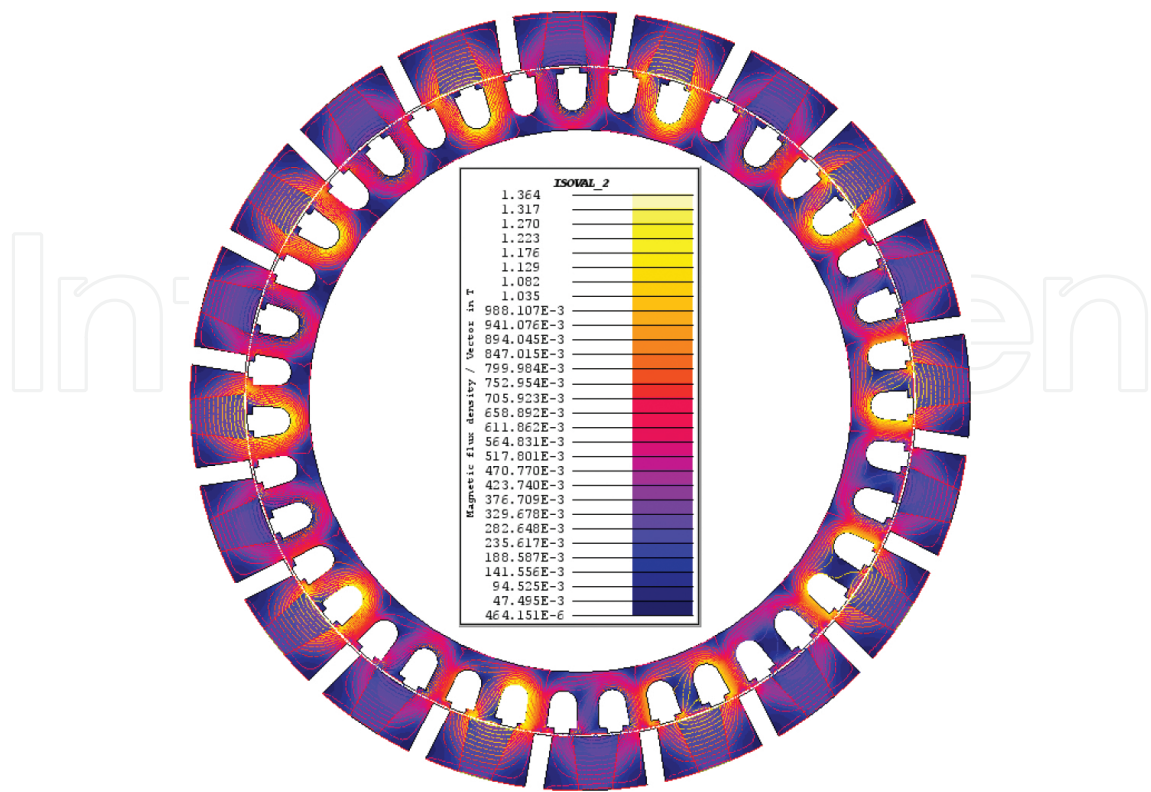


Figure 19. Flux density and field lines for studied PMSMOR.

The saturation level can be shown in **Figure 19**. It can be observed that the maximum value is almost 1.3 T in stator teeth. Because this value is below the maximum saturation level, more optimization can be performed in order to reduce the stator and rotor core.

In the next step of the simulation, the generator has been tested in load condition at rated power (3 kW) and speed.

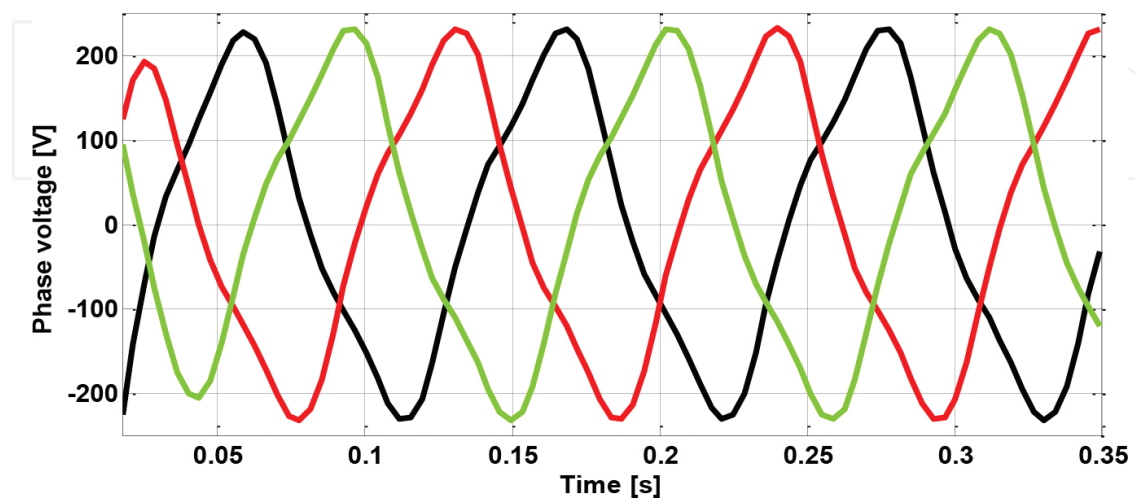


Figure 20. Computed voltage (rms value) at rated power.

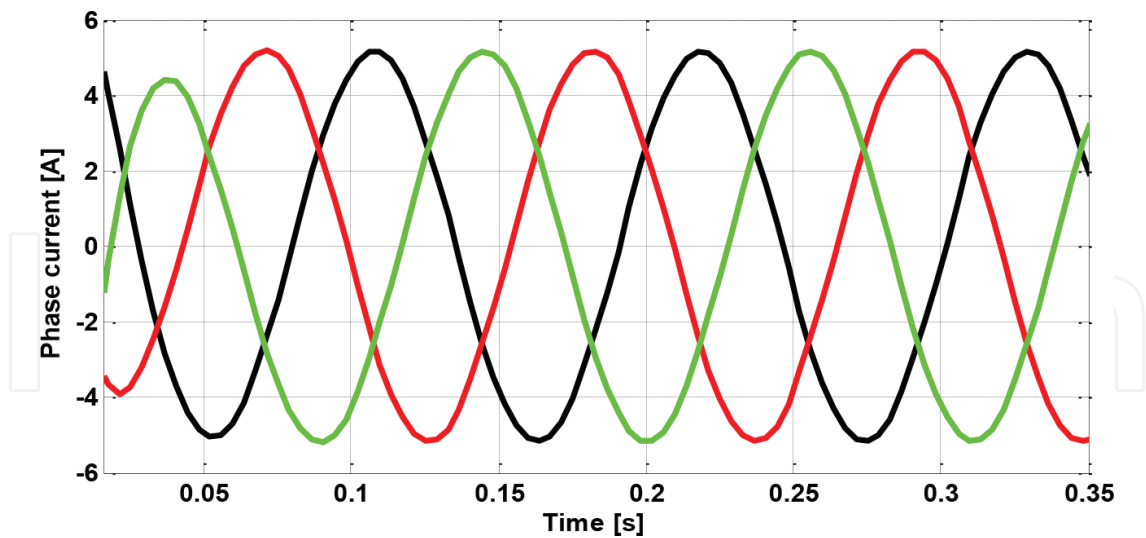


Figure 21. Computed current (rms value) at rated power.

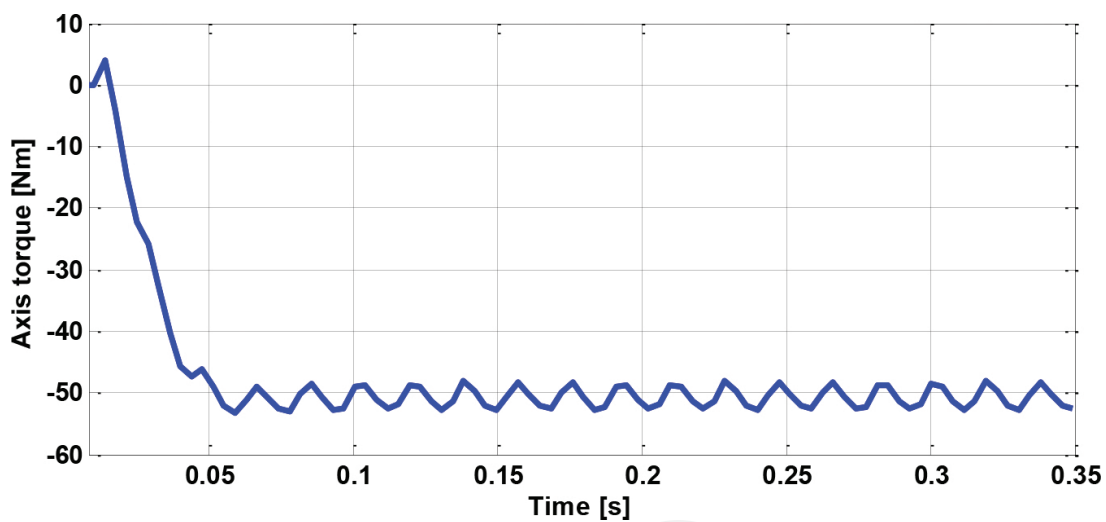


Figure 22. Axis torque in generator regime.

The generated phase voltage and obtained phase current using resistive load have been plotted in **Figures 20** and **21**, respectively. The average values of voltage and current are 223 V and 5.12 A, respectively, very close to the ones obtained from the analytical approach. The rated torque depicted in **Figure 22** is obtained for the rated current. Also, thanks to the proper winding–slots–poles combinations, the torque ripples are significantly reduced. In fact, the ratio of torque ripple is 6.6% (maximum at 52.5 Nm and minimum at 49.1 Nm).

3.3. Generators steady-state performances

In order to obtain the complete evaluation of performances of considered generators, an analysis in load condition was carried out for three different driven speeds for each generator.

3.3.1. Steady-state performances of PMCPSPG

The simulation of PMCPSPG has been performed for three different speeds: 500, 750, and 1000 rpm. The efficiency, the generated voltage, and the electric power have been computed, but the additional losses were neglected.

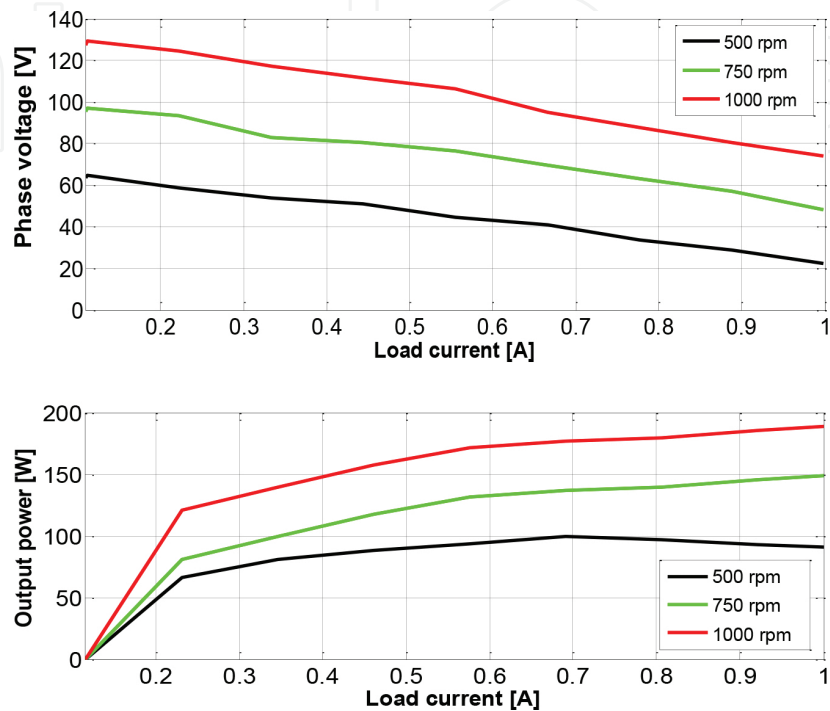


Figure 23. Steady-state performance of PMCPSPG: phase voltage and output power.

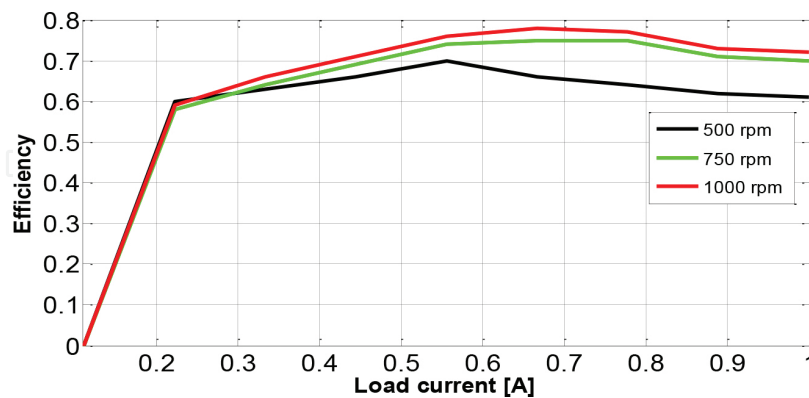


Figure 24. Steady-state performance of PMCPSPG.

Figures 23 and 24, respectively, show the steady-state performance (terminal voltage, output power, and efficiency) of the PMCPSPG supplying a resistive load. The voltage-current characteristics are approximately linear from no load to rated load. Due to the rather high armature impedance, the voltage drop difference between no load and rated load is of 57% at

750 rpm. As it can be noted, for low speeds, the maximum efficiency occurs at rather low values of load current. For higher speeds, the load current for which the maximum efficiency is obtained is increasing.

3.3.2. Steady-state performances of PMSMOR

The simulation of PMSMOR has been performed for three different speeds: 250, 500, and 750 rpm.

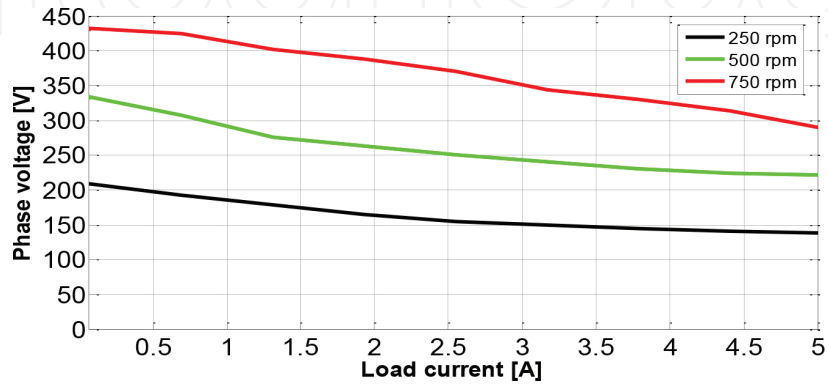


Figure 25. Performance of PMSMOR: phase voltage.

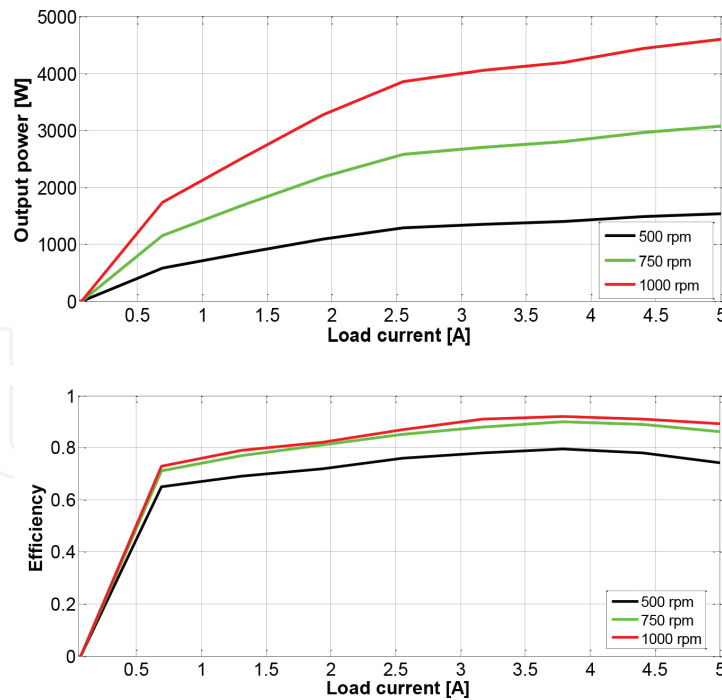


Figure 26. Performance of PMSMOR: output power and efficiency.

The voltage–current characteristics of PMSMOR are depicted in **Figure 25**. Also, the voltage drop difference between no load and rated load at 500 rpm is of 42%. The efficiency of the

generator can be shown in **Figure 26**. It can be observed that the maximum value is 0.92 for 3.62 A and 1000 rpm.

4. Conclusions

This chapter presents the main steps to be followed in the design of a low-cost permanent magnet synchronous machine suitable for small rating, direct driven applications, such as small- and microscale wind power plants. The analytical approach contains the major elements which need to be discussed. Detailed equations are presented for the calculation of geometrical parameters corresponding to the chosen special topologies of the rotor (claw pole and outer rotor). Also, the output performances (generated voltages, efficiency, losses) of the generators were computed. After preliminary design of the generators, the optimization procedure was performed using Hooke-Jeeves algorithm, in order to obtain the final topologies of the rotor in condition of maximum: efficiency, terminal voltage, and optimum weight.

The static performance of the machine, phase voltage, output power, and efficiency at different values of speed in order to obtain more detailed information, was studied through numerical analysis using Flux 3D for PMCSPG and 2D for PMSMOR.

Acknowledgements

This research work was supported by DDesign, Modelling and TESTing tools for Electrical Vehicles (DEMOTEST) project, in the frame of FP7 IAPP Marie Curie Actions.

Author details

Florin-Nicolae Jurca

Address all correspondence to: florin.jurca@emd.utcluj.ro

Department of Electrical Machines and Drives, Technical University of Cluj-Napoca, Cluj-Napoca, Romania

References

- [1] Bang D, Polinder H, Shrestha G, Ferreira JA. Review of generator systems for direct-drive wind turbines. In: Proceedings of the European Wind Energy Conference and Exhibition (EWEC '08); 31 March 2008, Brussels, Belgium, p. 1800–1810.

- [2] Camara MS, Camara MB, Dakyo B, Gualous H. Permanent magnet synchronous generator for offshore wind energy system connected to grid and battery-modelling and control strategies. *Int J Renew Energy*. 2015;2:386–393.
- [3] Latoufis KC, Messinis GM, Kotsampopouls PC, Hatziargyriou ND. Axial flux permanent magnet generator design for low cost manufacturing of small wind turbines. *Wind Eng*. 2012;4:411–431. doi:10.1260/0309-524X.36.4.411.
- [4] Pyrhonen J, Jokinen T, Hrabocova V. *Design of rotating electrical machines*. New York: Wiley; 2008. p. 538. doi:10.1002/9780470740095.
- [5] Hendershot JR, Miller TJE. *Design of brushless permanent-magnet motors*. Oxford: Magna Physics Publishing and Clarendon; 1994. p. 584.
- [6] Jurca FN, Martis C. Theoretical and experimental analysis of a three-phase permanent magnet claw-pole synchronous generator. *IET Electr Power Appl*. 2012; 6: 491–503. doi: 10.1049/iet-epa.2012.0075.
- [7] Gieras JF. *Permanent magnet motor technology*. Design Appl. New York: M. Dekker; 1997.
- [8] Jurca FN, Martis C. Claw-pole generator parameters and steady-state performances analysis. *Int Rev Model Simul*. 2013.
- [9] Boldea I. *Synchronous generators*. Boca Raton: CRC Press Taylor&Francis. 2006. p. 444.
- [10] Lundmark SKT. *Application of 3-D computation of magnetic fields to the design of claw pole motors [thesis]* Goteborg: Chalmers University of Technology, 2005.
- [11] Hembach H, Gerling D, Beyer S. Estimation of boundaries for the claw-pole geometry in electrical water pump applications. In: *Proceedings of the International Conference on Electrical Machines [ICEM '06]: 12–14 April 2007; Setubal, Portugal, 2007*, p. 174–179.
- [12] Permanent Magnet Datasheet [Internet]. <http://www.eclipsemagnetics.com>. Accessed: 2015-12-04.
- [13] Fodorean D, Djerdir A, Viorel I.A, Miraoui A. A double excited synchronous machine for direct drive application-design and prototype test. *IEEE Trans Energy Conv*. 2007;22:656–665. doi:10.1109/TEC.2007.896279.
- [14] Jurca F.N, Martis C, Birou I, Biro K, Analysis of permanent magnet claw-pole synchronous machine. In: *Proceedings of the international conference on optimization of electrical and electronics equipment, [OPTIM '08]: 19–20 May 2008, Brasov, Romania*, p. 75–80.